Analytical Formulation of Supermodes in Multicore Fibers With Hexagonally Distributed Cores
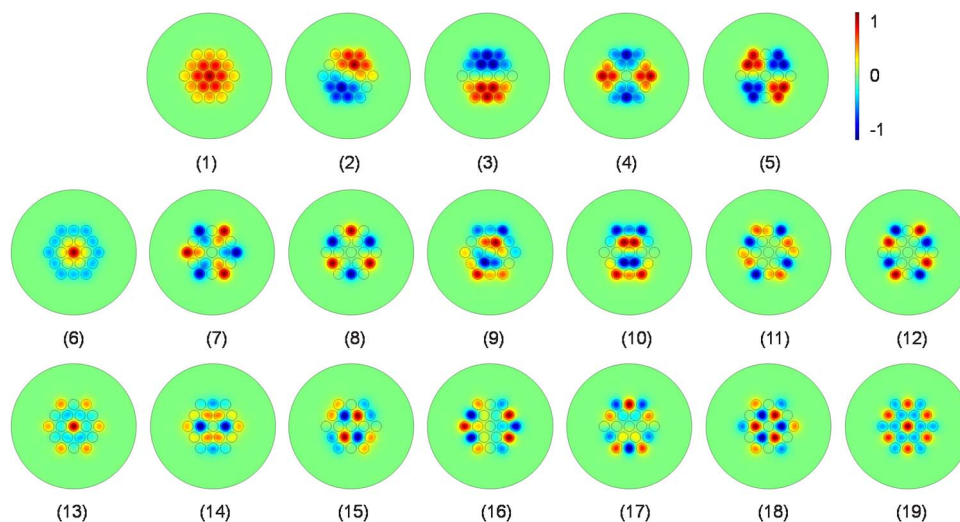
Wenhua Ren
Zhongwei Tan
Guobin Ren

Analytical Formulation of Supermodes in Multicore Fibers With Hexagonally Distributed Cores

Wenhua Ren,[1,2] **Zhongwei Tan,**[1] **and Guobin Ren**[1]

[1]Institute of Lightwave Technology, Key Laboratory of All Optical Network and Advanced Telecommunication Network of EMC, Beijing Jiaotong University, Beijing 100044, China
[2]Electrical Engineering Department, University of California Los Angeles, Los Angeles, CA 90095 USA

Abstract: The supermodes in 19-core multicore fibers (MCFs) with identical hexagonally distributed cores are analyzed in detail by using the coupled mode theory and matrix operation. The analytical formulations for both the propagation constants and modal distribution vectors of the supermodes are derived. Simulation results show that the analytical results agree well with the numerical results. In addition, the features of the effective indices and modal distributions of the supermodes are discussed by using the analytical expressions combined with the applications. The analytical expressions provide a fast and accurate method to reveal the properties and characteristics of the supermodes for MCFs and are helpful for the design and applications of MCFs.

Index Terms: Multicore fibers (MCFs), supermodes.

1. Introduction

Multicore fibers (MCFs) can be widely used in optical communication systems [1]–[6], fiber lasers [7]–[10], fiber couplers [11], fiber sensors [12]–[14], fiber endoscopes [15]–[17], microwave photonics [18], etc. The super-modes, whose electrical field distribution will not vary along the fiber length, are the eigen modes of MCFs and are greatly useful in the understanding and analysis of the properties of MCFs [19]. What's more, the super-modes themselves also can be used directly in optical communication systems and fiber lasers. For example, the mode-division multiplexing (MDM) by using the super-modes of MCFs has been proposed to increase the fiber capacity [2]–[5]. Also the super-modes in MCF lasers have been used to achieve high quality and high power laser [7]–[10]. Consequently, an intensive study of the super-modes is quite significant and necessary for the analysis, design, and applications of MCFs.

The super-modes of MCFs can be analyzed by using either numerical simulations [5], [20], [21] or analytical methods [4], [11], [22]–[25]. Comparing with numerical simulation results, the analytical results can give a deeper insight into the properties and characteristics of the super-modes. They can be used to analyze behaviors of the super-modes fast and completely [4], [5]. Currently, quite a few analytical results for the super-modes of MCFs have been derived,
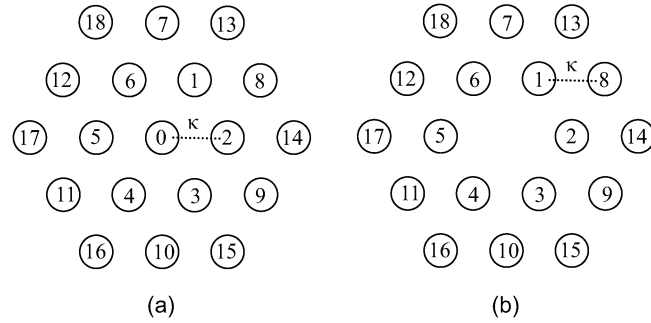
Fig. 1. Cross-section of the (a) 19-core and (b) 18-core MCFs with hexagonally distributed cores and the coupling coefficient.

including MCFs with linear aligned cores [22], circularly aligned cores within one ring [11], [23], two rings [24], and multi rings [25]. In [24] and [25], the adjacent rings are assumed to have the same number of cores, and each core in one ring is only coupled with one special core in the adjacent ring. However, in practice, the cores of MCFs are generally distributed in a hexagonal pattern, since it is the densest two-dimensional distribution and suitable for dense MCF design, e.g., 7 cores, 19 cores, 37 cores, etc. [7]–[9], [20], [21]. This kind of core distribution is different from that in previous papers [24], [25], and the corresponding super-modes have not been analyzed.

In this paper, our research focus on the analysis of the super-modes in MCFs with hexagonally distributed cores. In Section 2, the super-modes in the 19-core MCFs with hexagonally distributed cores are analyzed by using the coupled mode theory (CMT) and matrix operation. The analytical expressions for both the propagation constants and modal distribution vectors of the super-modes are derived. In Section 3, the analytical expressions are verified by comparing with the full vector finite element method (FEM). Simulation results show that the analytical results agree well with the numerical results. Also, the feature of effective indices and the modal distributions of the super-modes are discussed by using the analytical expressions, which are not easy to be obtained only by using the numerical method. The method described in this paper is a general method for super-modes analysis in MCFs with hexagonally distributed cores, and can be extended to multi-layer hexagonally distributed cores situations naturally.

It should be mentioned that in the following analysis, we only consider the coupling between adjacent cores and assume that each core of the MCF only supports single mode.

2. Super-Modes in 19-Core MCFs With Hexagonally Distributed Cores

Fig. 1(a) shows the cross-section of the 19-core MCF with hexagonally distributed cores. All the cores are identical and are ordered as in Fig. 1. According to the conclusions in [23], [25], some super-modes in this kind of MCFs are the same as those in 18-core MCFs with hexagonally distributed cores [see Fig. 1(b)], but the appearance of the center core will bring changes to the remaining super-modes. In this section, our analysis will start from the 18-core MCFs and will then consider the changes brought by the center core.

2.1. Super-Modes in 18-Core MCFs With Hexagonally Distributed Cores

In Fig. 1(b), the 18 cores are divided into three groups as cores 1–6, cores 7–12, and cores 13–18. The adjacent cores have the same core-to-core distance and coupling coefficient κ. Here the coupling coefficient is assumed to be real, which is true in most practical cases [26]. If the mode field of each fiber is $a_k \exp(-i\beta z)$, where a_k is the amplitude of the field at the kth core and β is the propagation constant of the single core in the absence of other cores, the propagation of the fields in each core can be described by using the CMT

$$\frac{d\mathbf{A}}{dz} = -i\mathbf{M}\mathbf{A} \tag{1}$$

where

$$\mathbf{A} = [\, a_1 \quad \cdots \quad a_{18}\,]^{\mathbf{T}}, \quad \mathbf{M} = \begin{bmatrix} \boldsymbol{\kappa_1} & \mathbf{C_{12}} & \mathbf{C_{13}} \\ \mathbf{C_{12}^{T}} & \mathbf{0} & \boldsymbol{\kappa_2} \\ \mathbf{C_{13}^{T}} & \boldsymbol{\kappa_2^{T}} & \mathbf{0} \end{bmatrix}_{18\times 18}, \quad \mathbf{C_{13}} = \begin{bmatrix} \kappa & & \\ & \ddots & \\ & & \kappa \end{bmatrix}_{6\times 6}$$

$$\boldsymbol{\kappa_1} = \begin{bmatrix} 0 & \kappa & & & \kappa \\ \kappa & 0 & \kappa & & \\ \ddots & \ddots & \ddots & & \\ & & \kappa & 0 & \kappa \\ \kappa & & & \kappa & 0 \end{bmatrix}_{6\times 6}, \quad \boldsymbol{\kappa_2} = \begin{bmatrix} \kappa & 0 & & & \kappa \\ \kappa & \kappa & 0 & & \\ \ddots & \ddots & \ddots & & \\ & & \kappa & \kappa & 0 \\ & & & \kappa & \kappa \end{bmatrix}_{6\times 6}, \quad \mathbf{C_{12}} = \begin{bmatrix} \kappa & \kappa & & & \\ 0 & \kappa & \kappa & & \\ \ddots & \ddots & \ddots & & \\ & & 0 & \kappa & \kappa \\ \kappa & & & 0 & \kappa \end{bmatrix}_{6\times 6}.$$

$$(2)$$

As seen from (2), $\boldsymbol{\kappa_1}$, $\boldsymbol{\kappa_2}$, $\mathbf{C_{12}}$, $\mathbf{C_{13}}$ are circulant matrices. According to the properties of the circulant matrix, they have different eigen values but have the same eigen vectors. In fact, they can be written as [25]

$$\boldsymbol{\kappa_1} = \mathbf{Q D_1 Q^{H}}, \quad \boldsymbol{\kappa_2} = \mathbf{Q D_2 Q^{H}}, \quad \mathbf{C_{12}} = \mathbf{Q D_{12} Q^{H}}, \quad \mathbf{C_{13}} = \mathbf{Q D_{13} Q^{H}} \tag{3}$$

where $\mathbf{D_1}$, $\mathbf{D_2}$, $\mathbf{D_{12}}$, $\mathbf{D_{13}}$ are diagonal matrices and their corresponding nth diagonal elements are

$$d_1^{(n)} = 2\kappa \cos\left[\frac{\pi(n-1)}{3}\right], \quad d_2^{(n)} = \kappa\left[1 + \exp\left(i\frac{\pi(n-1)}{3}\right)\right]$$

$$d_{12}^{(n)} = \kappa\left[1 + \exp\left(-i\frac{\pi(n-1)}{3}\right)\right], \quad d_{13}^{(n)} = \kappa. \tag{4}$$

Here, the columns of the matrix $\mathbf{Q}$ are the normalized orthogonal eigen vectors whose elements are

$$Q_{mn} = \frac{1}{\sqrt{6}}\exp\left[-i\frac{(m-1)(n-1)\pi}{3}\right] \tag{5}$$

and the superscript "H" denotes Hermitian operation.

Hence, the total coupling matrix can be written as

$$\mathbf{M} = \mathbf{Q_{total}} \begin{bmatrix} \mathbf{D_1} & \mathbf{D_{12}} & \mathbf{D_{13}} \\ \mathbf{D_{12}^{*}} & \mathbf{0} & \mathbf{D_2} \\ \mathbf{D_{13}^{*}} & \mathbf{D_2^{*}} & \mathbf{0} \end{bmatrix} \mathbf{Q_{total}^{H}}, \quad \mathbf{Q_{total}} = \begin{bmatrix} \mathbf{Q} & \mathbf{0} & \mathbf{0} \\ \mathbf{0} & \mathbf{Q} & \mathbf{0} \\ \mathbf{0} & \mathbf{0} & \mathbf{Q} \end{bmatrix} \tag{6}$$

where the superscript "*" denotes conjugate operation. Furthermore, the matrix in the middle of (6) can be decomposed into

$$\begin{bmatrix} \mathbf{D_1} & \mathbf{D_{12}} & \mathbf{D_{13}} \\ \mathbf{D_{12}^{*}} & \mathbf{0} & \mathbf{D_2} \\ \mathbf{D_{13}^{*}} & \mathbf{D_2^{*}} & \mathbf{0} \end{bmatrix} = \mathbf{UNU} \tag{7}$$

where

$$\mathbf{N} = \begin{bmatrix} d_1^{(1)} & d_{12}^{(1)} & d_{13}^{(1)} & & & & \\ d_{12}^{(1)*} & 0 & d_2^{(1)} & & & & \\ d_{13}^{(1)} & d_2^{(1)*} & 0 & & & & \\ & & & \ddots & & & \\ & & & & d_1^{(6)} & d_{12}^{(6)} & d_{13}^{(6)} \\ & & & & d_{12}^{(6)*} & 0 & d_2^{(6)} \\ & & & & d_{13}^{(6)} & d_2^{(6)*} & 0 \end{bmatrix} \tag{8}$$

and matrix $\mathbf{U}$ is a matrix which originates from the row exchange of the identity matrix [25].

The matrix $\mathbf{N}$ is a Hermitian matrix, i.e., $\mathbf{N} = \mathbf{N^H}$, so it can be further decomposed into

$$\mathbf{N} = \mathbf{V\Lambda V^H} \tag{9}$$

where the diagonal matrix $\mathbf{\Lambda}$ has the elements corresponding to the eigen values of $\mathbf{M}$ and $\mathbf{N}$, and its $(3n-2)$th element, $(3n-1)$th element, and $(3n)$th element are the eigen values of the nth sub-matrix of the matrix $\mathbf{N}$. In fact, they are the three roots of the following equation:

$$\lambda^3 + A\lambda^2 + B\lambda + C = 0$$

$$A = -d_1^{(n)} = -2\kappa\cos\left(\frac{n-1}{3}\pi\right), \quad B = -\left|d_2^{(n)}\right|^2 - \left|d_{12}^{(n)}\right|^2 - \left|d_{13}^{(n)}\right|^2 = -\kappa^2\left[5 + 4\cos\left(\frac{n-1}{3}\pi\right)\right]$$

$$C = d_1^{(n)}\left|d_2^{(n)}\right|^2 - d_{13}^{(n)}\left[d_2^{(n)}d_{12}^{(n)} + \left(d_2^{(n)}d_{12}^{(n)}\right)^*\right] = 4\kappa^3\left[\cos\left(\frac{n-1}{3}\pi\right) - 1\right]\left[\cos\left(\frac{n-1}{3}\pi\right) + 1\right] \tag{10}$$

where $n = 1, 2, \cdots, 6$. The roots of (10) can be shown to be

$$\lambda_k^{(n)} = \begin{cases} (1+\sqrt{10})\kappa, 0, (1-\sqrt{10})\kappa & n=1 \\ 3.354\kappa, -0.477\kappa, -1.877\kappa & n=2,6 \\ \sqrt{3}\kappa, -\kappa, -\sqrt{3}\kappa & n=3,5 \\ (\sqrt{2}-1)\kappa, 0, -(\sqrt{2}+1)\kappa & n=4 \end{cases} \tag{11}$$

where $k = 1, 2, 3$ and the three corresponding eigen vectors are

$$\begin{bmatrix} \mathbf{x_k^{(1)}} \\ \mathbf{x_k^{(2)}} \\ \mathbf{x_k^{(3)}} \\ \mathbf{x_k^{(4)}} \\ \mathbf{x_k^{(5)}} \\ \mathbf{x_k^{(6)}} \end{bmatrix} = \begin{cases} [0.712, 0.551, 0.436]^T, \frac{[2,-1,-2]^T}{3}, [-0.222, 0.765, -0.605]^T \\ [0.642, 0.508+0.293i, 0.494]^T, [0.719, -0.204-0.118i, -0.654]^T \\ [-0.268, 0.671+0.388i, -0.573]^T \\ \frac{[2(\sqrt{3}-1), 1+\sqrt{3}i, 2]^T}{\sqrt{24-8\sqrt{3}}}, \frac{[0, 1+\sqrt{3}i, -2]^T}{2\sqrt{2}}, \frac{[-2(1+\sqrt{3}), 1+\sqrt{3}i, 2]^T}{\sqrt{24-8\sqrt{3}}} \\ \frac{[1, 0, \sqrt{2}+1]^T}{\sqrt{4+2\sqrt{2}}}, [0, 1, 0]^T, \frac{[\sqrt{2}+1, 0, -1]^T}{\sqrt{4+2\sqrt{2}}} \\ \mathbf{x_k^{(3)*}} \\ \mathbf{x_k^{(2)*}}. \end{cases} \tag{12}$$

Then, the matrix $\mathbf{V}$ is just formed by the block matrices, i.e., all the $\mathbf{x_k^{(n)}}$.

Hence, all the propagation constants for the 18-core MCFs are

$$\beta + \lambda_k^{(n)}. \tag{13}$$

The total eigen vectors of the matrix $\mathbf{M}$, whose columns will be the modal distribution vectors for super-modes, can be obtained by using $\mathbf{W} = \mathbf{Q_{total}UV}$. The modal distribution vector corresponds to the $\beta + \lambda_k^{(n)}$ can be shown to be

$$\mathbf{W_p} = \left[\mathbf{x_k^{(n)}}(1)\mathbf{q_n^T}, \quad \mathbf{x_k^{(n)}}(2)\mathbf{q_n^T}, \quad \mathbf{x_k^{(n)}}(3)\mathbf{q_n^T}\right]^T, \qquad p = 3(n-1)+k \tag{14}$$

where $\mathbf{q_n}$ is the nth column of the matrix $\mathbf{Q}$, and $\mathbf{W_p}$ is the pth column of the matrix $\mathbf{W}$.

Normally, the mode amplitudes a_k are real-valued, so the elements of the matrix $\mathbf{W}$ should be chosen to be real-valued. From (11), we know that the propagation constants of nth group modes and $(8-n)$th group modes are the same, i.e., they are degenerate. Therefore, we can use the following expressions:

$$\mathbf{W_p} = \begin{cases} \left[\mathbf{x_k^{(n)}}(1)\mathbf{q_n^T}, \mathbf{x_k^{(n)}}(2)\mathbf{q_n^T}, \mathbf{x_k^{(n)}}(3)\mathbf{q_n^T}\right]^T, & n=1,4 \\ \sqrt{2}\left[\mathbf{x_k^{(n)}}(1)\mathrm{Re}\{\mathbf{q_n^T}\}, \mathrm{Re}\{\mathbf{x_k^{(n)}}(2)\mathbf{q_n^T}\}, \mathbf{x_k^{(n)}}(3)\mathrm{Re}\{\mathbf{q_n^T}\}\right]^T, & n=2,3 \\ \sqrt{2}\left[\mathbf{x_k^{(n)}}(1)\mathrm{Im}\{\mathbf{q_n^T}\}, \mathrm{Im}\{\mathbf{x_k^{(n)}}(2)\mathbf{q_n^T}\}, \mathbf{x_k^{(n)}}(3)\mathrm{Im}\{\mathbf{q_n^T}\}\right]^T, & n=5,6 \end{cases} \begin{pmatrix} k=1,2,3 \\ p=3(n-1)+k \end{pmatrix}. \tag{15}$$

2.2. Super-Modes in 19-Core MCFs With Hexagonally Distributed Cores

Comparing with 18-core MCFs with hexagonally distributed cores, there is one more center core for 19-core MCFs, as shown in Fig. 1(a). There will be coupling between the center core and surrounding 6 cores.

The coupling matrix for 19-core MCFs will be

$$
\mathbf{M} = \begin{bmatrix} \mathbf{0} & \mathbf{b} & \mathbf{0} & \mathbf{0} \\ \mathbf{b}^{\mathsf{T}} & \boldsymbol{\kappa}_1 & \mathbf{C}_{12} & \mathbf{C}_{13} \\ \mathbf{0} & \mathbf{C}_{12}^{\mathsf{T}} & \mathbf{0} & \boldsymbol{\kappa}_2 \\ \mathbf{0} & \mathbf{C}_{13}^{\mathsf{T}} & \boldsymbol{\kappa}_2^{\mathsf{T}} & \mathbf{0} \end{bmatrix}_{19 \times 19}
\tag{16}
$$

where $\mathbf{b} = \kappa[1,1,1,1,1,1]_{1\times 6}$ stands for the coupling between the center core and surrounding six cores.

According to the conclusion in [23], the matrix

$$
\mathbf{M}_1 = \begin{bmatrix} \mathbf{0} & \mathbf{b} \\ \mathbf{b}^{\mathsf{T}} & \boldsymbol{\kappa}_1 \end{bmatrix}_{7 \times 7}
\tag{17}
$$

has seven eigen values, five of which are the same as those of the matrix $\boldsymbol{\kappa}_1$, and the corresponding eigen vectors remain the same except for an additional component with value 0. However, the first eigen value $d_1^{(1)}$ will be replaced by

$$
d_1^{'(0)} = (1 - \sqrt{7})\kappa, \quad d_1^{'(1)} = (1 + \sqrt{7})\kappa
\tag{18}
$$

and the corresponding eigen vectors are

$$
\mathbf{q}_0' = \frac{1}{\sqrt{14 + 2\sqrt{7}}}[-1 - \sqrt{7}, 1, 1, 1, 1, 1, 1]^{\mathsf{T}}, \quad \mathbf{q}_1' = \frac{1}{\sqrt{14 - 2\sqrt{7}}}[-1 + \sqrt{7}, 1, 1, 1, 1, 1, 1]^{\mathsf{T}}.
\tag{19}
$$

The matrix $\mathbf{M}_1$ can be written as $\mathbf{M}_1 = \mathbf{Q}'\mathbf{D}_1'\mathbf{Q}'^{\mathsf{H}}$, where the diagonal elements of the diagonal matrix $\mathbf{D}_1'$ are the eigen values of the matrix $\mathbf{M}_1$ and the columns of the matrix $\mathbf{Q}'$ are the corresponding eigen vectors.

Therefore, the matrix $\mathbf{M}$ can be written as

$$
\mathbf{M} = \begin{bmatrix} \mathbf{Q}' & & \\ & \mathbf{Q} & \\ & & \mathbf{Q} \end{bmatrix} \begin{bmatrix} \mathbf{D}_1' & \mathbf{D}_{12}' & \mathbf{D}_{13}' \\ \mathbf{D}_{12}'^* & \mathbf{0} & \mathbf{D}_2 \\ \mathbf{D}_{13}'^* & \mathbf{D}_2^* & \mathbf{0} \end{bmatrix} \begin{bmatrix} \mathbf{Q}' & & \\ & \mathbf{Q} & \\ & & \mathbf{Q} \end{bmatrix}^{\mathsf{H}} = \mathbf{Q}_{\text{total}}' \begin{bmatrix} \mathbf{D}_1' & \mathbf{D}_{12}' & \mathbf{D}_{13}' \\ \mathbf{D}_{12}'^* & \mathbf{0} & \mathbf{D}_2 \\ \mathbf{D}_{13}'^* & \mathbf{D}_2^* & \mathbf{0} \end{bmatrix} \mathbf{Q}_{\text{total}}'^{\mathsf{H}}
\tag{20}
$$

where

$$
\mathbf{D}_{12}' = \mathbf{Q}'^{\mathsf{H}} \begin{bmatrix} \mathbf{0} \\ \mathbf{C}_{12} \end{bmatrix} \mathbf{Q} = \begin{bmatrix} d_{12}'^{(0)} & & & \cdots & & 0 \\ & d_{12}'^{(1)} & & \cdots & & 0 \\ & & d_{12}^{(2)} & & & \\ \vdots & & & \ddots & & \\ 0 & & & & & d_{12}^{(6)} \end{bmatrix}, \quad
\mathbf{D}_{13}' = \mathbf{Q}'^{\mathsf{H}} \begin{bmatrix} \mathbf{0} \\ \mathbf{C}_{13} \end{bmatrix} \mathbf{Q} = \begin{bmatrix} d_{13}'^{(0)} & & & \cdots & & 0 \\ & d_{13}'^{(1)} & & \cdots & & 0 \\ & & d_{13}^{(2)} & & & \\ \vdots & & & \ddots & & \\ 0 & & & & & d_{13}^{(6)} \end{bmatrix}
$$

$$
d_{12}'^{(0)} = \sqrt{\frac{3}{7 + \sqrt{7}}} \cdot 2\kappa, \quad d_{12}'^{(1)} = \sqrt{\frac{3}{7 - \sqrt{7}}} \cdot 2\kappa, \quad d_{13}'^{(0)} = \sqrt{\frac{3}{7 + \sqrt{7}}} \cdot \kappa, \quad d_{13}'^{(1)} = \sqrt{\frac{3}{7 - \sqrt{7}}} \cdot \kappa
\tag{21}
$$

and other elements can be calculated by using (4).

By using the same method as (7)–(9), the matrix in the center of (20) can be decomposed into $\mathbf{M} = \mathbf{U}\mathbf{N}\mathbf{U}^{\mathsf{H}} = \mathbf{U}\mathbf{V}\boldsymbol{\Lambda}\mathbf{V}^{\mathsf{H}}\mathbf{U}^{\mathsf{H}}$, where the matrix $\mathbf{N}$ has the same block matrices as in (8) for

$n = 2, \ldots, 6$, while the first block matrix is

$$
\begin{bmatrix}
d_1^{\prime(0)} & 0 & d_{12}^{\prime(0)} & d_{13}^{\prime(0)} \\
0 & d_1^{\prime(1)} & d_{12}^{\prime(1)} & d_{13}^{\prime(1)} \\
d_{12}^{\prime(0)} & d_{12}^{\prime(1)} & 0 & d_2^{(1)} \\
d_{13}^{\prime(0)} & d_{13}^{\prime(1)} & d_2^{(1)} & 0
\end{bmatrix}. \tag{22}
$$

From (22), we can obtain four eigen values

$$
\lambda_s^{(1)} = 4.872\kappa, \; 1.227\kappa, \; -1.622\kappa, \; -2.477\kappa, \qquad s = 1, 2, 3, 4 \tag{23}
$$

and the corresponding eigen vectors are

$$
\mathbf{x}_s^{(1)} = [0.104, 0.826, 0.443, 0.334]^\mathsf{T}, [-0.310, 0.548, -0.504, -0.591]^\mathsf{T}
$$
$$
[-0.679, 0.005, -0.340, 0.651]^\mathsf{T}, [-0.657, -0.133, 0.660, -0.340]^\mathsf{T}. \tag{24}
$$

The total eigen vectors of the matrix $\mathbf{M}$, whose columns will be the modal distribution vectors for super-modes, can be obtained by using $\mathbf{W} = \mathbf{Q}'_{\mathbf{total}}\mathbf{UV}$. By using the same method as (14) and (15), we can obtain the modal distribution vectors for 19-core MCFs:

$$
\mathbf{W_p} =
\begin{cases}
\left[\mathbf{x}_s^{(1)}(1)\mathbf{q}_0^{\prime\mathsf{T}} + \mathbf{x}_s^{(1)}(2)\mathbf{q}_1^{\prime\mathsf{T}}, \mathbf{x}_s^{(1)}(3)\mathbf{q}_1^\mathsf{T}, \mathbf{x}_s^{(1)}(4)\mathbf{q}_1^\mathsf{T} \right]^\mathsf{T}, & n=1 \quad (s=1,2,3,4 \quad p=s) \\[2mm]
\sqrt{2}\left[0, \mathbf{x}_k^{(n)}(1)\mathrm{Re}\{\mathbf{q}_n^\mathsf{T}\}, \mathrm{Re}\{\mathbf{x}_k^{(n)}(2)\mathbf{q}_n^\mathsf{T}\}, \mathbf{x}_k^{(n)}(3)\mathrm{Re}\{\mathbf{q}_n^\mathsf{T}\} \right]^\mathsf{T}, & n=2,3 \\[2mm]
\left[0, \mathbf{x}_k^{(4)}(1)\mathbf{q}_4^\mathsf{T}, \mathbf{x}_k^{(4)}(2)\mathbf{q}_4^\mathsf{T}, \mathbf{x}_k^{(4)}(3)\mathbf{q}_4^\mathsf{T} \right]^\mathsf{T}, & n=4 \quad \left(\begin{matrix} k=1,2,3 \\ p=3n+k-2 \end{matrix} \right) \\[2mm]
\sqrt{2}\left[0, \mathbf{x}_k^{(n)}(1)\mathrm{Im}\{\mathbf{q}_n^\mathsf{T}\}, \mathrm{Im}\{\mathbf{x}_k^{(n)}(2)\mathbf{q}_n^\mathsf{T}\}, \mathbf{x}_k^{(n)}(3)\mathrm{Im}\{\mathbf{q}_n^\mathsf{T}\} \right]^\mathsf{T}, & n=5,6
\end{cases}
$$
$$
\tag{25}
$$

where $\mathbf{x}_s^{(1)}$ and $\mathbf{x}_k^{(n)}$ are from (24) and (12), $\mathbf{q}'_0$ and $\mathbf{q}'_1$ are from (19), and $\mathbf{q_n}$ is the nth column of the matrix $\mathbf{Q}$, which can be calculated by using (5).

Here, we summarize the propagation constants and modal distribution vectors for all the super-modes in 19-core MCFs with hexagonally distributed cores in Table 1. The modes are rearranged by using the propagation constants.

3. Simulation and Discussion

The propagation constant β and effective index n_{eff} are two key parameters for the super-modes in MCFs. The propagation constants can be used to calculate the intermodal beat lengths, group delay spread and mode-dependent chromatic dispersion of the super-modes, which are three of the most important properties of MCFs for MDM [5]. The effective indices determine the number of propagating modes and the bending loss of each mode [4]. According to $\beta = 2\pi n_{eff}/\lambda$, where λ is the wavelength, the effective indices for the super-modes can be calculated by using the propagation constant expressions in Table 1.

The modal distribution is also an important characteristic for the super-modes, which determines the effective area of the super-modes relating to the nonlinear properties of MCFs [4], [5].

To verify the theory in Section 2, here we calculate the effective indices and modal distributions of the super-modes in 19-core MCFs with identical hexagonally distributed cores, by using both the analytical expressions obtained in Section 2 and the full vector FEM, which is a precise numerical method that can test the precision of the analytical results.

3.1. The Effective Index

As seen from Table 1, there are 19 super-modes (or 38 modes if we consider the polarization modes) in the 19-core MCFs, and some of them are degenerate. If we take the 19 cores as a

TABLE 1

Propagation constants and modal distribution vectors for the super-modes in 19-core MCFs

Mode number	Propagation constants	Modal distribution vectors	Notes	Corresponding LP modes
1	$\beta + 4.872\kappa$	$\left[x_s^{(1)}(1)q_0^{'T} + x_s^{(1)}(2)q_1^{'T}, x_s^{(1)}(3)q_1^T, x_s^{(1)}(4)q_1^T\right]^T$	$s=1$	LP$_{01}$
2	$\beta + 3.354\kappa$	$\sqrt{2}\left[0, x_k^{(m)}(1)\mathrm{Re}\{q_n^T\}, \mathrm{Re}\{x_k^{(m)}(2)q_n^T\}, x_k^{(m)}(3)\mathrm{Re}\{q_n^T\}\right]^T$	$n=2,k=1$	LP$_{11}$
3		$\sqrt{2}\left[0, x_k^{(m)}(1)\mathrm{Im}\{q_n^T\}, \mathrm{Im}\{x_k^{(m)}(2)q_n^T\}, x_k^{(m)}(3)\mathrm{Im}\{q_n^T\}\right]^T$	$n=6,k=1$	
4	$\beta + \sqrt{3}\kappa$	$\sqrt{2}\left[0, x_k^{(m)}(1)\mathrm{Re}\{q_n^T\}, \mathrm{Re}\{x_k^{(m)}(2)q_n^T\}, x_k^{(m)}(3)\mathrm{Re}\{q_n^T\}\right]^T$	$n=3,k=1$	LP$_{21}$
5		$\sqrt{2}\left[0, x_k^{(m)}(1)\mathrm{Im}\{q_n^T\}, \mathrm{Im}\{x_k^{(m)}(2)q_n^T\}, x_k^{(m)}(3)\mathrm{Im}\{q_n^T\}\right]^T$	$n=5,k=1$	
6	$\beta + 1.227\kappa$	$\left[x_s^{(1)}(1)q_0^{'T} + x_s^{(1)}(2)q_1^{'T}, x_s^{(1)}(3)q_1^T, x_s^{(1)}(4)q_1^T\right]^T$	$s=2$	LP$_{02}$
7	$\beta + (\sqrt{2}-1)\kappa$	$\left[0, x_k^{(4)}(1)q_4^T, x_k^{(4)}(2)q_4^T, x_k^{(4)}(3)q_4^T\right]^T$	$n=4,k=1$	LP$_{31}$
8	β		$n=4,k=2$	
9	$\beta - 0.477\kappa$	$\sqrt{2}\left[0, x_k^{(m)}(1)\mathrm{Re}\{q_n^T\}, \mathrm{Re}\{x_k^{(m)}(2)q_n^T\}, x_k^{(m)}(3)\mathrm{Re}\{q_n^T\}\right]^T$	$n=2,k=2$	LP$_{12}$
10		$\sqrt{2}\left[0, x_k^{(m)}(1)\mathrm{Im}\{q_n^T\}, \mathrm{Im}\{x_k^{(m)}(2)q_n^T\}, x_k^{(m)}(3)\mathrm{Im}\{q_n^T\}\right]^T$	$n=6,k=2$	
11	$\beta - \kappa$	$\sqrt{2}\left[0, x_k^{(m)}(1)\mathrm{Re}\{q_n^T\}, \mathrm{Re}\{x_k^{(m)}(2)q_n^T\}, x_k^{(m)}(3)\mathrm{Re}\{q_n^T\}\right]^T$	$n=3,k=2$	LP$_{41}$
12		$\sqrt{2}\left[0, x_k^{(m)}(1)\mathrm{Im}\{q_n^T\}, \mathrm{Im}\{x_k^{(m)}(2)q_n^T\}, x_k^{(m)}(3)\mathrm{Im}\{q_n^T\}\right]^T$	$n=5,k=2$	
13	$\beta - 1.622\kappa$	$\left[x_s^{(1)}(1)q_0^{'T} + x_s^{(1)}(2)q_1^{'T}, x_s^{(1)}(3)q_1^T, x_s^{(1)}(4)q_1^T\right]^T$	$s=3$	LP$_{03}$
14	$\beta - \sqrt{3}\kappa$	$\sqrt{2}\left[0, x_k^{(m)}(1)\mathrm{Re}\{q_n^T\}, \mathrm{Re}\{x_k^{(m)}(2)q_n^T\}, x_k^{(m)}(3)\mathrm{Re}\{q_n^T\}\right]^T$	$n=3,k=3$	LP$_{22}$
15		$\sqrt{2}\left[0, x_k^{(m)}(1)\mathrm{Im}\{q_n^T\}, \mathrm{Im}\{x_k^{(m)}(2)q_n^T\}, x_k^{(m)}(3)\mathrm{Im}\{q_n^T\}\right]^T$	$n=5,k=3$	
16	$\beta - 1.877\kappa$	$\sqrt{2}\left[0, x_k^{(m)}(1)\mathrm{Re}\{q_n^T\}, \mathrm{Re}\{x_k^{(m)}(2)q_n^T\}, x_k^{(m)}(3)\mathrm{Re}\{q_n^T\}\right]^T$	$n=2,k=3$	LP$_{51}$
17		$\sqrt{2}\left[0, x_k^{(m)}(1)\mathrm{Im}\{q_n^T\}, \mathrm{Im}\{x_k^{(m)}(2)q_n^T\}, x_k^{(m)}(3)\mathrm{Im}\{q_n^T\}\right]^T$	$n=6,k=3$	
18	$\beta - (1+\sqrt{2})\kappa$	$\left[0, x_k^{(4)}(1)q_4^T, x_k^{(4)}(2)q_4^T, x_k^{(4)}(3)q_4^T\right]^T$	$n=4,k=3$	LP$_{32}$
19	$\beta - 2.477\kappa$	$\left[x_s^{(1)}(1)q_0^{'T} + x_s^{(1)}(2)q_1^{'T}, x_s^{(1)}(3)q_1^T, x_s^{(1)}(4)q_1^T\right]^T$	$s=4$	LP$_{04}$

whole, the modal distributions of the super-modes are similar to that in a single core fiber. Most of MCFs are weakly guiding optical fibers, so the modes can be treated as linearly polarized modes (LP modes). The 1st super-mode is the fundamental mode, i.e. LP$_{01}$ mode (degenerate HE$_{11}$ modes), which has the largest effective index; The second and third super-modes will degenerate to LP$_{11}$ mode (degenerate TE$_{01}$, TM$_{01}$, HE$_{21}$ modes); The fourth and fifth super-modes will degenerate to LP$_{21}$ mode (degenerate EH$_{11}$, HE$_{31}$ modes). All the rest of the super-modes are associated with corresponding LP modes. In total, the 19 super-modes can be classified as 12 LP modes, which have been shown in Table 1.

The polarization is also one of the important characteristics of super-modes. In fact, every super-mode consists of two independent polarization modes. The degenerate super-modes (as shown in Table 1) consist of four independent polarization modes. For instance, the 6th super-mode in Table 1 consists of two independent polarization modes, which corresponds to LP$_{02}$ mode. The degenerate second and third super-modes in Table 1 consists of four independent polarization modes, which corresponds to LP$_{11}$ mode.

Here we choose three super-modes to carry out the calculation: the LP$_{01}$ mode with the largest effective index, the LP$_{31}$ mode with a normal propagation constant β, and the LP$_{04}$ mode with the smallest effective index. We calculated the effective indices of the super-modes under different gap sizes (edge-to-edge distance between adjacent cores), core diameters, and relative index differences. The simulation results are plotted in Fig. 2.
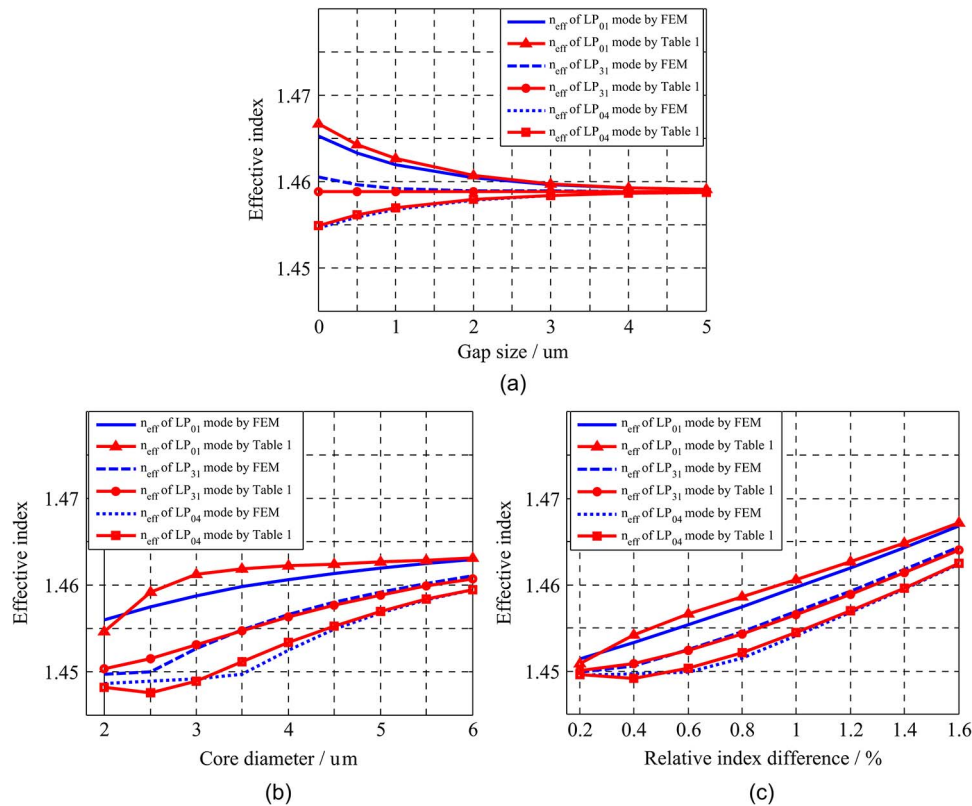
Fig. 2. (a) Effective indices of the super-modes vary with the gap size, with a core radius 2.5 μm, cladding index 1.45, relative index difference 1.2%, working wavelength 1.55 um, which are the same with previous papers [4], [25], [28]. (b) Effective indices of the super-modes vary with the core diameter, with a gap size 1 um. (c) Effective indices of the super-modes vary with the relative index difference; the others are the same with (a).

As seen from Fig. 2, the effective indices calculated by using the analytical expressions in Table 1 match well with the FEM results in all simulations. Even for the case of strong coupling among cores, e.g., when the gap size is zero, or the core diameter and the relative index difference is quite small, the error between the results is less than 0.2%.

Also we can see that the effective index of the LP_{04} mode is less than the cladding index 1.45 when the core diameter or the relative index difference is small, which means the LP_{04} mode has been cut off. In fact, sometimes we hope to reduce the number of modes in the MCFs to few modes or even single-mode operation in practice [4], [9]. This can be realized by adjusting fiber parameters. From the expressions in Table 1, it seems that we can obtain the conclusion that the super-modes with a propagation constant less than β are easy to be cut off, and the remaining 5 LP modes will not be cut off forever. But this conclusion is not always true.

As seen from Fig. 2, when the core diameter or the relative index difference is quite small, the fiber core cannot limit the light well and the effective indices will be close to the cladding index. In this case, the calculation error between the analytical results and numerical results may lead to an error result when calculating the number of propagating modes, even though the error is quite small. For example, for a 19-core fiber with a core diameter 2 um, gap size 3.5 um, cladding index 1.45, relative index difference 0.17%, and working wavelength 1.05 um, most of which are from [9], [27] but with a different relative index difference, the FEM simulation results shows that only the fundamental mode (LP_{01} mode) existing in the fiber, which means that the LP_{11}, LP_{21}, LP_{02}, and LP_{31} modes are cut off. But the analytical expressions cannot predict this result. For the calculation error, one reason is when the core diameter or relative index difference or the gap size is quite small, there will be strong coupling among cores. In this case, the
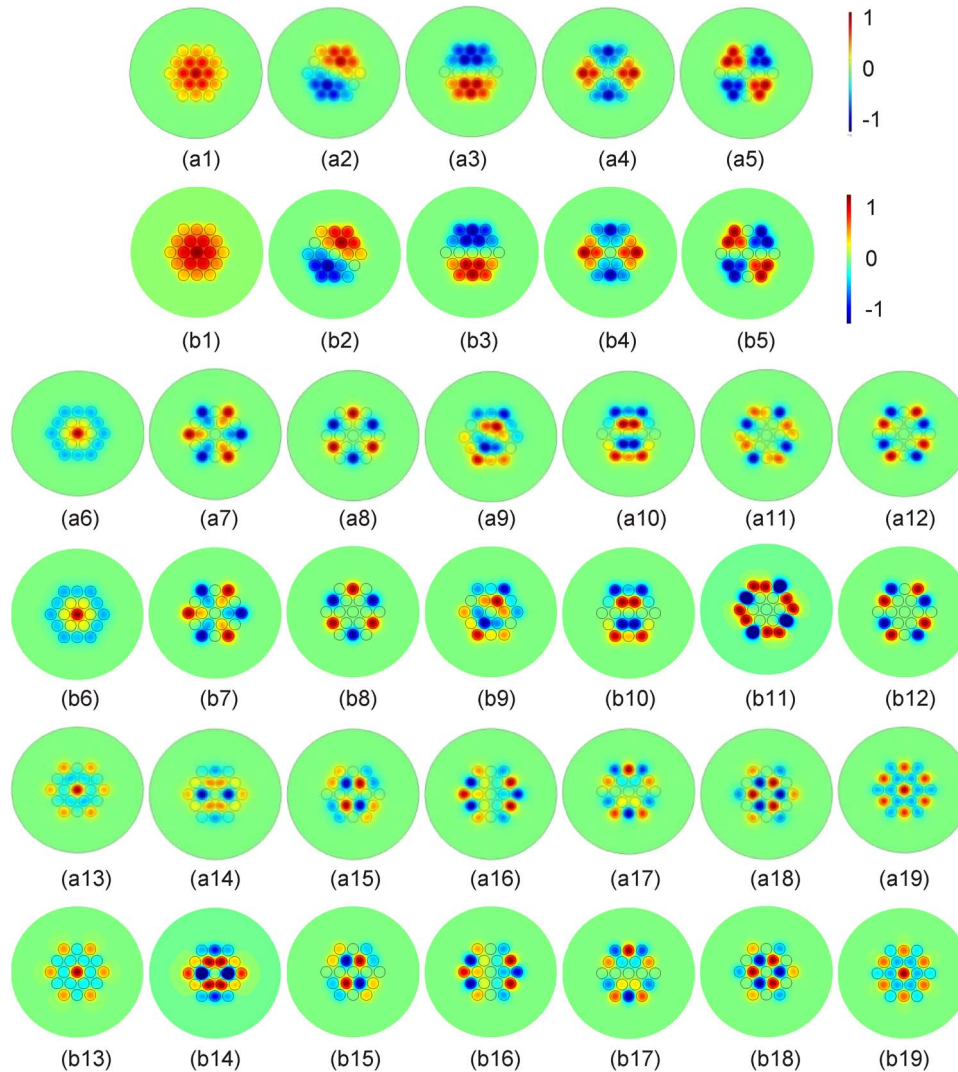
Fig. 3. Modal distributions of all the super-modes in 19-core MCFs with hexagonally distributed cores. (a1)–(a19) are obtained by using FEM, and (b1)–(b19) are corresponding results obtained by using the analytical expressions.

coupling between nonadjacent cores need to be taken into account. Therefore, the analytical expressions in Table 1 should be utilized carefully for this kind of fiber. However, those modes with effective indices too close to the cladding index cannot be transmitted efficiently in the fiber, and can be cut off easily. In fact, for such weakly guided modes, no intentional perturbations would be needed to induce cut off—loose coiling and unintentional perturbations would be enough [27]. For this reason, the small calculation error is not a serious disadvantage.

3.2. The Modal Distribution

We calculated the modal distributions of all the super-modes in 19-core MCFs with hexagonally distributed cores by using the FEM and the analytical expressions in Table 1 or (25), respectively. The results are shown in Fig. 3. The fiber parameters are set as: core diameter 5 um, gap size 1 um, cladding index 1.45, and relative index difference 1.2%, which are the same as previous papers [4], [21], [24]. In Fig. 3, (a1)–(a19) are obtained by using FEM, and (b1)–(b19) are corresponding results obtained by using the analytical expressions in Table 1. As seen from Fig. 3, the modal distributions obtained by analytical expressions agree well with numerical results.

TABLE 2

Correlation coefficients between the analytical results and the numerical results for the modal distribution

Mode Number	Correlation coefficients	Mode Number	Correlation coefficients	Mode Number	Correlation coefficients
1	0.998	8	0.992	15	0.990
2	0.988	9	0.976	16	0.992
3	0.996	10	0.989	17	0.992
4	0.994	11	0.979	18	0.992
5	0.994	12	0.989	19	0.990
6	0.993	13	0.979		
7	0.990	14	0.990		

In addition, the analytical expressions of the modal distribution can give a deeper insight into the characteristics of the super-modes and provide more information. Firstly, the surrounding 18-cores can be divided into three groups as cores 1–6, cores 7–12, cores 13–18, as in Fig. 1. According to (25), each group has the same modal distribution as the super-modes in 6-core MCFs with hexagonally distributed cores, but the amplitude will be modulated by $\mathbf{x}_s^{(1)}$ and $\mathbf{x}_k^{(n)}$. Secondly, among the 19 super-modes plotted in Fig. 3, only four modes (the LP_{01}, LP_{02}, LP_{03}, LP_{04} modes) have significant modal amplitude in the center core. For the rest of the 15 modal distributions, the modal amplitudes in the center core are zero. In other words, the appearance of the center core only affects four LP modes and the rest of the modes just remain the same as those in 18-core MCFs. Third, as seen from (12), some elements of $\mathbf{x}_k^{(n)}$ are zero, e.g., $\mathbf{x}_2^{(3)}$, $\mathbf{x}_2^{(5)}$, $\mathbf{x}_1^{(4)}$, $\mathbf{x}_2^{(4)}$, $\mathbf{x}_3^{(4)}$, so the modal amplitude in corresponding group (including six cores) will be zero, i.e. 7th, 8th (LP_{31}), 11th, 12th (LP_{41}), 18th (LP_{32}) modes in Table 1. All these features are confirmed in Fig. 3.

In order to further verify the modal distribution by using the analytical expressions, here, we define the correlation coefficient as

$$R_{cc} = \frac{\iint_S E_1 E_2 \, ds}{\iint_S E_1^2 \, ds} \tag{26}$$

where E_1, E_2 are electrical field distributions obtained by using the FEM and (25), and have been normalized by using the total power, respectively. The correlation coefficient directly shows the similarity between the analytical result and the numerical result. By using (26), we obtained the correlation coefficients for all the 19 super-modes, which are listed in the Table 2. The mode orders are the same as those in Table 1.

As seen from the Table 2, the correlation coefficients for all the super-modes are more than 0.97, which means that the modal distribution obtained by using the analytical expressions in (25) are excellent agreement with the numerical results.

4. Conclusion

In this paper, we have analyzed the super-modes in 19-core MCFs with identical hexagonally distributed cores by using the CMT. The analytical expressions for both the propagation constants and modal distribution vectors of the super-modes are derived. Furthermore, we calculated the effective indices and the modal distributions of the super-modes by using the analytical expressions and the numerical method, respectively. Simulation results show that the analytical results agree quite well with the numerical results. Additionally, the effective indices and the modal distribution features of the super-modes are discussed by using the analytical expressions, which are not easy to be obtained only by using the numerical method. The method can also be extended to multi-layer hexagonally distributed cores situations naturally.

The analytical expressions provide a more complete understanding of the super-modes in the MCFs and will be helpful for the analysis, design, and applications of MCFs.

Acknowledgment

References

[1] R.-J. Essiambre, R. Ryf, N. K. Fontaine, and A. Randel, "Breakthroughs in photonics 2012: Space-division multiplexing in multimode and multicore fibers for high-capacity optical communication," *IEEE Photon. J.*, vol. 5, no. 2, Apr. 2013, Art. ID. 0701307.

[2] D. J. Richardson, J. M. Fini, and L. E. Nelson, "Space-division multiplexing in optical fibres," *Nature Photon.*, vol. 7, no. 5, pp. 354–362, May 2013.

[3] Y. Kokubun and M. Koshiba, "Novel multi-core fibers for mode division multiplexing: Proposal and design principle," *IEICE Electron. Exp.*, vol. 6, no. 8, pp. 522–528, Apr. 2009.

[4] C. Xia, N. Bai, I. Ozdur, X. Zhou, and G. Li, "Supermodes for optical transmission," *Opt. Exp.*, vol. 19, no. 17, pp. 16 653–16 664, Aug. 2011.

[5] S. O. Arik and J. M. Kahn, "Coupled-core multi-core fibers for spatial multiplexing," *IEEE Photon. Technol. Lett.*, vol. 25, no. 21, pp. 2054–2057, Nov. 2013.

[6] R. G. H. van Uden *et al.*, "Ultra-high-density spatial division multiplexing with a few-mode multicore fibre," *Nature Photon.*, vol. 8, no. 11, pp. 865–870, Nov. 2014.

[7] C. Jollivet *et al.*, "Mode-resolved gain analysis and lasing in multi-supermode multi-core fiber laser," *Opt. Exp.*, vol. 22, no. 24, pp. 30 377–30 386, Nov. 2014.

[8] Y. Huo, P. Cheo, and G. King, "Fundamental mode operation of a 19-core phase-locked Yb-doped fiber amplifier," *Opt. Exp.*, vol. 12, no. 25, pp. 6230–6239, Dec. 2004.

[9] M. M. Vogel, M. Abdou-Ahmed, A. Voss, and T. Graf, "Very-large-mode-area, single-mode multicore fiber," *Opt. Lett.*, vol. 34, no. 18, pp. 2876–2878, Sep. 2009.

[10] P. Zhou *et al.*, "Beam quality and power scalability of various multicore fiber lasers," *Chin. Phys. Lett.*, vol. 26, no. 8, Aug. 2009, Art. ID. 084205.

[11] J. Hudgings, L. Molter, and M. Dutta, "Design and modeling of passive optical switches and power dividers using non-planar coupled fiber arrays," *IEEE J. Quantum Electron.*, vol. 36, no. 12, pp. 1438–1444, Dec. 2000.

[12] L. B. Yuan and X. Wang, "Four-beam single fiber optic interferometer and its sensing," *Sens. Actuators A*, vol. 138, no. 1, pp. 9–15, Jul. 2007.

[13] Z. Y. Zhao *et al.*, "All-solid multi-core fiber-based multipath Mach-Zehnder interferometer for temperature sensing," *Appl. Phys. B-Lasers Opt.*, vol. 112, no. 4, pp. 491–497, Sep. 2013.

[14] G. Salceda, A. Van Newkirk, J. E. Antonio-Lopez, A. Schulzgen, and R. Amezcua-Correa, "Optical fiber curvature sensors based on single mode-7 core-single mode fiber structures," in *Advanced Photonics*, OSA Tech. Dig. (online), Washington, DC, USA, Paper SeW3C.2.

[15] A. F. Gmitro and D. Aziz, "Confocal microscopy through a fiber-optic imaging bundle," *Opt. Lett.*, vol. 18, no. 8, pp. 565–567, Apr. 1993.

[16] W. Göbel, J. N. D. Kerr, A. Nimmerjahn, and F. Helmchen, "Miniaturized two-photon microscope based on a flexible coherent fiber bundle and a gradient-index lens objective," *Opt. Lett.*, vol. 29, no. 21, pp. 2521–2523, Nov. 2004.

[17] K. L. Reichenbach and C. Xu, "Numerical analysis of light propagation in image fibers or coherent fiber bundles," *Opt. Exp.*, vol. 15, no. 5, pp. 2151–2165, Mar. 2007.

[18] I. Gasulla and J. Capmany, "Microwave photonics applications of multicore fibers," *IEEE Photon. J.*, vol. 4, no. 3, pp. 877–888, Jun. 2012.

[19] G. P. Agrawal, *Applications of Nonlinear Fiber Optics.*   San Diego, CA, USA: Academic, 2001.

[20] A. Mafi and J. Moloney, "Shaping modes in multicore photonic crystal fibers," *IEEE Photon. Technol. Lett.*, vol. 17, no. 2, pp. 348–350, Feb. 2005.

[21] Y. Zheng *et al.*, "Supermode analysis in multi-core photonic crystal fiber laser," in *Proc. SPIE*, 2010, 7843, Art. ID. 784316.

[22] C. Y. Guan, L. B. Yuan, Q. Dai, and F. J. Tian, "Supermodes analysis for linear-core-array microstructured fiber," *J. Lightw. Technol.*, vol. 27, no. 11, pp. 1741–1745, May 2009.

[23] S. Peleš, J. L. Rogers, and K. Wiesenfeld, "Robust synchronization in fiber laser arrays," *Phys. Rev. E Statist. Nonlinear Softw. Matter Phys.*, vol. 73, no. 2, Feb. 2006, Art. ID. 026212.

[24] C. N. Alexeyev, T. A. Fadeyeva, N. A. Boklag, and M. A. Yavorsky, "Supermodes of a double-ring fibre array with symmetric coupling," *Ukrainian J. Phys. Opt.*, vol. 12, no. 2, pp. 83–88, Feb. 2011.

[25] J Zhou, "Analytical formulation of super-modes inside multi-core fibers with circularly distributed cores," *Opt. Exp.*, vol. 22, no. 1, pp. 673–688, Jan. 2014.

[26] K. Okamoto, *Fundamentals of Optical Waveguides*.   San Diego, CA, USA: Academic, 2000.

[27] J. M. Fini, "Large-mode-area multicore fibers in the single-moded regime," *Opt. Exp.*, vol. 19, no. 5, pp. 4042–4046, Feb. 2011.

[28] F. Saitoh, K. Saitoh, and M. Koshiba, "A design method of a fiber-based mode multi/demultiplexer for mode-division multiplexing," *Opt. Exp.*, vol. 18, no. 5, pp. 4709–4716, Mar. 2010.